Sensors and Actuators A 162 (2010) 36–50

Contents lists available at ScienceDirect

Sensors and Actuators A: Physical

journal homepage: www.elsevier.com/locate/sna

Influence of amplitude and frequency modulation on flow created by a synthetic jet actuator

Adnan Qayoum, Vaibhav Gupta, P.K. Panigrahi *, K. Muralidhar

Department of Mechanical Engineering, Indian Institute of Technology Kanpur, Kanpur 208016, India

ARTICLE INFO

Article history:
Received 11 July 2009
Received in revised form 22 February 2010
Accepted 13 May 2010
Available online 17 June 2010

Keywords:
Synthetic jet
Piezoelectric actuator
Laser schlieren
Amplitude modulation
Frequency modulation
Active flow control

ABSTRACT

Synthetic jet actuator is a compact device that has applications in drag reduction, heat transfer enhancement and controlled mixing. An isolated synthetic jet is produced by the interaction of a train of vortices that are formed by alternate ejection and suction of fluid across an orifice such that the time-averaged mass flux is zero. A unique feature of a synthetic jet is that it is formed entirely from the working fluid of the flow system in which it is utilized. The temporal and spatial characteristics of the synthetic jet are dependent on the actuator operating conditions. Amplitude and frequency modulation of the actuator offer possibility of better flow control. No systematic study on the effect of amplitude modulation on synthetic jet characteristics is available in the literature. The present study reports the properties of the synthetic jet as a function of both excitation voltage and modulation frequency. Three modulating frequencies namely, 10 Hz, 25 Hz, and 50 Hz and excitation voltages in the range 5–50 V has been considered. Schlieren visualization has been used to characterize the jet spread while hotwire anemometry provides detailed time-averaged and fluctuating velocity fields. The present study shows a significant impact of amplitude modulation on the spatial and temporal evolution of synthetic jets. The rms velocity fluctuations increase due to amplitude modulation and the effect is more pronounced at low modulating frequencies. The behavior of a synthetic jet in the presence of a neighboring synthetic jet, i.e. the behavior of a dual synthetic jet configuration has also been investigated. The spreading of the jet is seen to increase considerably in the presence of a second neighboring synthetic jet.

1. Introduction

Synthetic jets have shown great promise as fluidic vortex generators in flow control, specifically, drag reduction and heat transfer enhancement applications. Synthetic jets are generated by the interactions of a train of vortices periodically drawn into and ejected from a cavity through an orifice. A typical synthetic jet actuator consists of an enclosed cavity with one or more openings (orifice or slot) on one side. The other face has a diaphragm for actuation. The oscillatory motion of the diaphragm leads to alternate suction and ejection of the fluid between the cavity and the cross-stream. During the suction stroke, the opening acts as a sink and entrains the near wall low momentum fluid into the cavity while during the expulsion stroke, a fluid jet accompanied by a train of vortices is formed. There is net momentum injection into the cross-stream without any additional mass addition. The literature related to the development and characterization of synthetic jets is presented below.

Smith and Glezer [1,2] prepared a high aspect ratio synthetic rectangular air jet and observed the time-harmonic formation and subsequent interactions of a train of counter-rotating vortex pairs. Even though the jet was formed without net mass injection, the hydrodynamic impulse of the ejected fluid and thus the momentum of the ensuing jet was non-zero. The authors found that successive vortex pairs were not subjected to pairing or other sub-harmonic interactions. In the far field, the synthetic jet was similar to conventional two-dimensional jets. However, in comparison to 2D jets, the streamwise reduction in the time-averaged centerline velocity of the synthetic jet was somewhat higher, while the streamwise width was lower.

Kral et al. [3] performed a two-dimensional numerical simulation of a synthetic jet. They modeled only the region outside the cavity with the actuation simulated using an analytical velocity profile at the orifice. Results obtained in their study confirmed the experimental observations of Smith and Glezer [1] only in the near-orifice region. Farther away from the orifice, the authors observed the vortex cores to be smeared by turbulent diffusion. In experiments, the vortices were seen to break down into a planar turbulent jet beyond 8–10 slot widths of the aperture. Rizzetta et al. [4] used DNS to solve the unsteady incompressible Navier–Stokes equations for flow generated by a synthetic

* Corresponding author. Tel.: +91 512 2597686; fax: +91 512 2597408.
E-mail address: panig@iitk.ac.in (P.K. Panigrahi).

0924-4247/$ – see front matter © 2010 Elsevier B.V. All rights reserved.
doi:10.1016/j.sna.2010.05.008

Nomenclature

D	orifice diameter of synthetic jet actuator (m)
E	anemometer output voltage (V)
l	orifice length (m)
L_0	stroke length (m)
PSD	power spectral density of the x-component of velocity fluctuation (m/s)
Re	Reynolds number based on orifice diameter and maximum velocity
V_{exc}	actuator excitation voltage (V)
u	velocity component in the x-direction (m/s)
u_{cl}	jet centerline velocity (m/s)
$u_0(t)$	instantaneous velocity at the orifice exit (m/s)
U_∞	free stream velocity (m/s)
u_{rms}	root mean square fluctuations of u-velocity (m/s)
t	time (s)
T	time period of one cycle(s)
S	Stokes number
x, y	Cartesian coordinates with x pointing in the direction of fluid ejection from the jet

Greek symbols

υ	kinematic viscosity (m^2/s)
ρ	fluid density (kg/m^3)

jet actuator. In addition to confirming the findings of Kral et al. [3], the authors also showed that flow in the internal cavity becomes periodic after several cycles. The breaking down of vortices into a turbulent jet was the result of three-dimensional flow instabilities which could not be captured in a two-dimensional simulation. These trends were confirmed by Mallinson et al. [5] who compared simulation against experiments with round jets.

Cater and Soria [6] experimentally investigated the spatial structure and time-averaged flow quantities of a round synthetic jet, generated by means of an oscillating piston in a cavity. Instantaneous velocity fields measured by means of particle image velocimetry showed radial entrainment in the near field and self-similarity in the far field. Three types, i.e. laminar, transitional and turbulent jets were observed with an increase in the jet Reynolds number.

Smith and Swift [7] conducted an experimental investigation of a continuous and a planar synthetic jet using schlieren imaging as well as hotwire anemometry. The Reynolds number (based on slot width and characteristic jet velocity) selected for the study was greater than 2000. The authors observed that synthetic jets are dominated by vortex pairs in the near field region that entrain more fluid than continuous jets and therefore grow rapidly in terms of jet width and volume flux. In the far field, both jets have self-similar velocity profiles.

Ugrina and Flatau [8] studied the effects of diaphragm type, cavity shape and nozzle geometry on the performance of the synthetic jet actuator. The authors observed that the performance of the synthetic jet actuator improves when the device is tuned such that the resonant frequency of the diaphragm matches with that of the cavity. Fugal et al. [9] numerically studied a two-dimensional synthetic jet and reported the effects of rounded and sharp exit section geometry. Cannelle and Amitay [10] studied the spatial evolution and transitory behavior of a planar synthetic jet using particle image velocimetry and hotwire anemometry. The authors observed the near-orifice vortex pairs to be uniform and two-dimensional that develop three-dimensionality in the downstream with the center moving faster than the sides. Trávníček et al. [11] studied a new fluid jet actuator consisting of a synthetic jet actuator and a valve-less pump. The resulting jet had an intrinsically non-zero-net-mass-flux, in contrast to a synthetic jet and was classified as hybrid. The actuator operated in a double-acting regime; both up- and down-strokes of the diaphragm forced the fluid to flow out from the central and the annular nozzles, respectively. A comparison between actuations by sine and square waves showed the sine-wave excitation of the diaphragm to be more effective.

Xu et al. [12] experimentally studied the instantaneous flow characteristics of a circular orifice synthetic jet by a phase-locked PIV system. The authors reported instantaneous flow fields, including the formation, development and breakdown of the vortex. Gaetano and Gaetano [13] investigated an axisymmetric synthetic jet produced by an oscillating piston with water as the working fluid using PIV. The authors showed that a single vortex ring or a train of vortex rings characterizes the near field during the blowing phase, depending on the jet properties leaving the orifice. Tesař and Kordík [14] developed a mathematical model for evaluating the spatial distributions of various quantities of interest in a synthetic jet. The approach was based on the similarity transformation that converts the governing equations (one equation for the time-mean momentum transport, the other for transport of energy of unsteady motion) into a set of simple ordinary equations. Instead of the asymptotic fully developed state, this approach employs the existing degree of freedom in the solution by varying, along the axial distance from the nozzle, a parameter which the transformed equations contain. The new quasi-similarity approach was found to agree very well with two experimentally investigated generic examples of synthetic jets.

Amplitude and frequency modulated flow control can target natural flow instabilities by introducing cross-flow perturbation at suitable frequencies that interact with the main flow. Hong [15] used a synthetic jet actuator in a laminar boundary layer as an instability trigger with stabilizing influence in an adverse pressure gradient flow. The author observed the synthetic jet actuator to be more effective at a lower critical frequency than at resonant frequency. The critical frequency was determined on considerations of flow instability (both T-S and K-H). The motivation for using the amplitude modulation actuation for synthetic jets comes from the natural demodulation of the high frequency carrier (the resonant frequency of the actuator) with the low frequency modulating signal that modifies the flow. This presents an opportunity to perturb the flow at non-resonant frequencies and thus adds flexibility in the design of an actuator. Few applications related to amplitude modulated synthetic jets are reviewed in the following paragraphs.

Ritchie and Seitzman [16] used amplitude modulated synthetic jets for active control of gaseous fuel–air mixing. The authors observed that amplitude modulation at lower frequencies creates large scale structures that persist downstream and have large effects on mixing, especially in the outer mixing layer. Rathnasingham and Breuer [17] used amplitude modulation to change the average velocity of the synthetic jet employed for active flow control in turbulent channel flow. Vukasinovic et al. [18] used amplitude-modulated actuation of synthetic jets for separation control over a hemispherical shell. Amplitude modulation was found to enhance phase-coherent large scale motions over a broad range of desirable frequencies. Margalit et al. [19] carried out a parametric study around a semi-span delta wing with a sharp leading edge using zero-mass-flux piezoelectric actuators operating at resonance with amplitude modulation and burst mode. High frequency unmodulated signal (pure sine waves) resulted in a slight degradation of the aerodynamic performance. The most significant aerodynamic

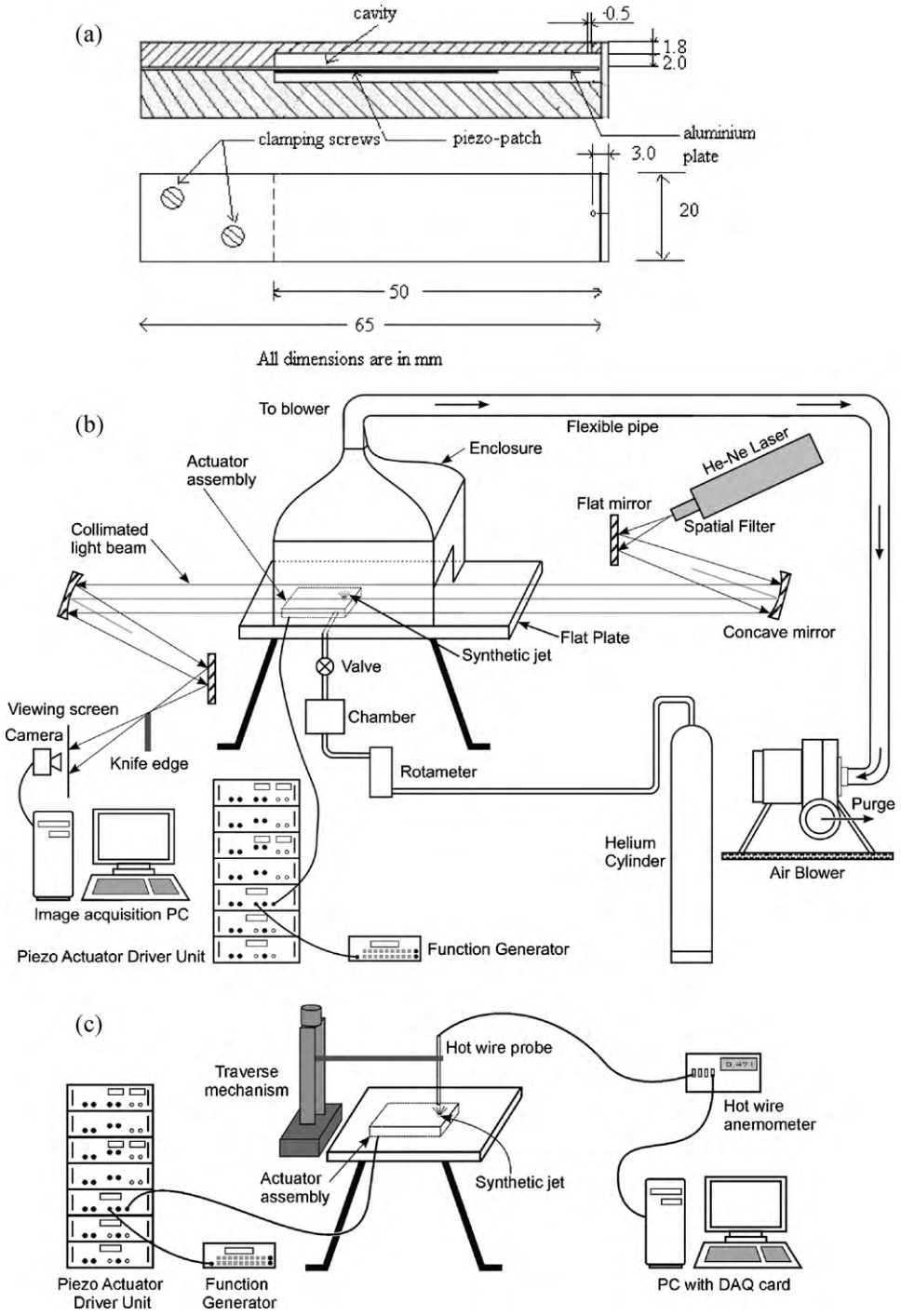

Fig. 1. (a) Schematic drawing of the synthetic jet actuator, (b) optical arrangement for schlieren visualization and (c) schematic of the setup for hot wire measurements.

enhancement was achieved for the burst mode with amplitude modulation.

The above literature review shows wide application of amplitude and frequency modulated synthetic jets in active flow control. However, the characterization of synthetic jet is limited to the unmodulated synthetic jet. There is no systematic study available in the literature on the influence of modulation on the synthetic jet characteristics. The objective of the present study is to investigate the influence of amplitude and frequency modulation on the flow characteristics of an isolated synthetic jet.

2. Experimental details

The experimental setup consists of the synthetic jet actuator, schlieren visualization facility, hotwire anemometry and the driver for piezo-actuation. The details of these components are described in the following sections.

2.1. Synthetic jet actuator

The synthetic jet actuator consists of an aluminum cantilever (50 mm × 20 mm × 0.4 mm) and a piezoelectric element (SP-5H

material measuring 40 mm × 19.75 mm × 0.4 mm) bonded to the cantilever near its support (Fig. 1(a)). The piezo-element is made of lead zirconate titanate and the electrical contacts to this element are provided by soldering the electrical leads to the terminals. The cantilever is enclosed from all sides with Plexiglas sheets forming a cavity. The top surface of the cavity has a circular orifice. Two orifice sizes of diameter 0.5 mm and 2 mm with a height of 1.8 mm have been used. The piezoelectric element oscillates when supplied with voltage signal from the function generator (Hewlett Packard HP 33120A) via an amplifier unit (Spranktronics). The highest amplitude of oscillation is obtained by exciting the piezo-element at the resonance frequency of the cantilever, namely 951 Hz for the present actuator. The synthetic jet actuator is used in ambient air and it entrains low momentum near wall air during the suction stroke. During expulsion, an air jet accompanied by train of vortices is formed.

2.2. Schlieren flow visualization

The spatial structure of the synthetic jet under different actuation conditions has been visualized using a monochrome schlieren technique as shown in Fig. 1(b). The Z-type 2-mirror schlieren system comprises of a continuous wave He–Ne laser light source (35 mW, 632.8 nm, Spectra-physics), a pair of flat and concave mirrors, a knife-edge and a viewing screen. The original laser beam is expanded by a spatial filter on to a concave mirror (f8, 160 mm focal length) guided by a flat mirror in-between. The collimated beam from the concave mirror passes through the test section

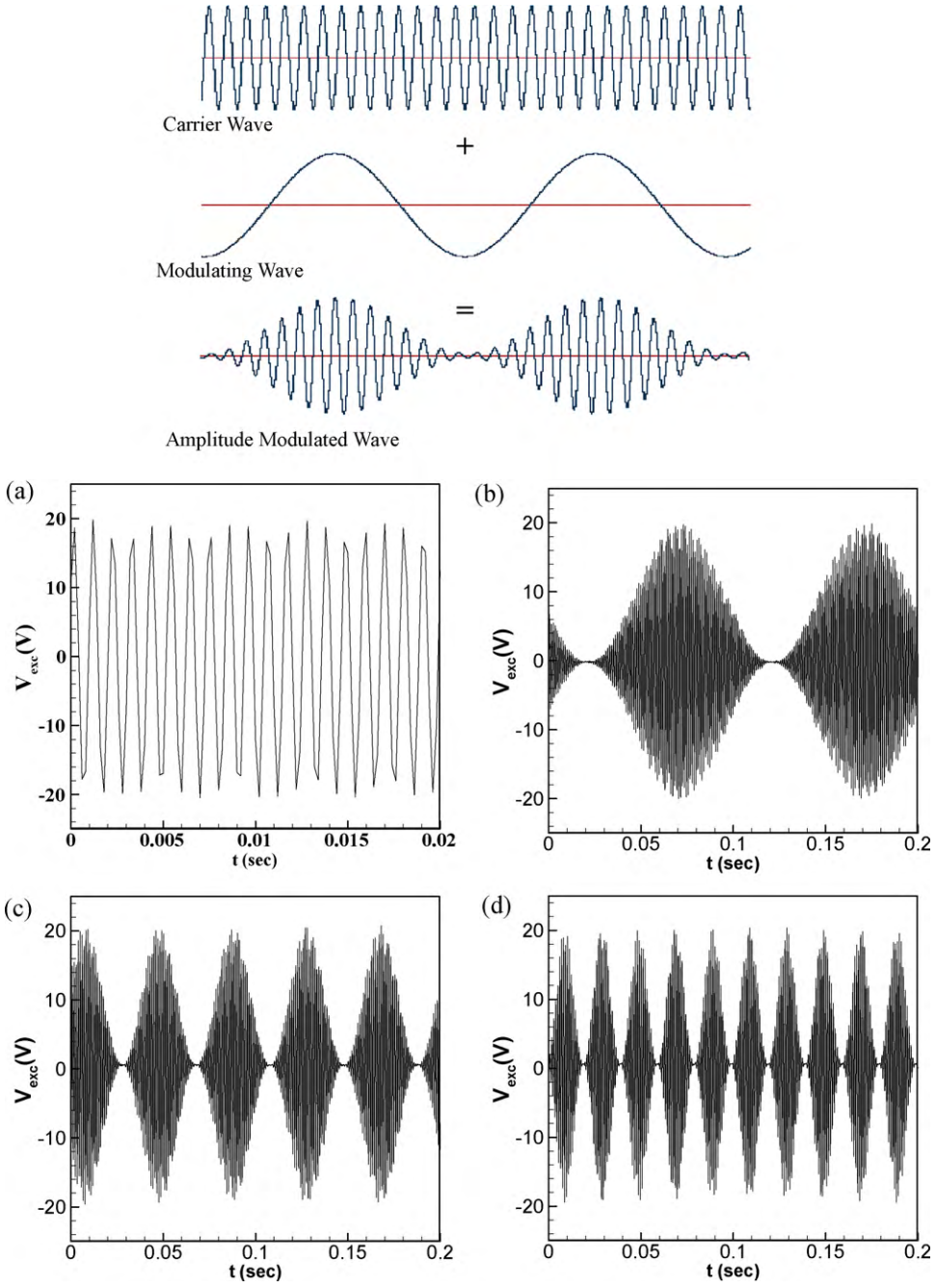

Fig. 2. The creation of an amplitude modulated signal and time traces for actuation voltage of ±20 V for the (a) unmodulated, (b) AM at f_{AM} = 10 Hz, (c) AM at f_{AM} = 25 Hz, and (d) AM at f_{AM} = 50 Hz.

and then to a second concave mirror (f8, 160 mm focal length) which refocuses the beam onto a knife-edge. The knife-edge is a razor blade, placed at the focal length of the second concave mirror.

The schlieren technique is sensitive to gradients in the refractive index field and hence, changes in the fluid density. To generate such gradients, helium has been used as a tracer element for visualization of the synthetic jet flow patterns. An arrangement is made for injecting helium in the cavity of the synthetic jet (Fig. 1(b)). The flow rate of helium is adjusted with the help of a rotameter to a small value, sufficient to fill the cavity, mix with air and create meaningful images on the screen. A high speed CMOS sensor based monochrome camera (MC1302, Mikrotron) with 8-bit dynamic resolution has been used to capture the sequence of schlieren images. The images are recorded at a speed of 250 frames per second with a spatial resolution of 512 × 512 pixels. The camera is connected to a PC-based image acquisition system through a 64-bit frame grabber card (X64-CL, Coreco Imaging).

2.3. Velocity measurement

Velocity measurements have been conducted under ambient conditions using a hotwire anemometer (CTA Bridge 56C17, Dantec) operating in the constant temperature mode (Fig. 1(c)). The hotwire anemometer is connected to a data acquisition card (Keithley KPCI 3108) and is run using LabView software. A single wire probe (55P11) is used for one-component velocity measurement. The hotwire probe is calibrated using a calibration apparatus (55D44, Dantec) and a pitot-static tube connected to a micromanometer (Furness Control, FC012). The hotwire location in both axial and radial directions is controlled by an automatic traverse connected to a personal computer. The sampling frequency is set equal to 5000 Hz with a sample size of 50,000 for each instantaneous velocity measurement.

2.4. Amplitude modulation

The piezoelectric patch mounted on the cantilever located inside the cavity of the synthetic jet actuator is of the resonant type. It generates the highest displacement at the cantilever resonant frequency. The resonant frequency of the cantilever is equal to 951 Hz, which is set as the carrier frequency for the amplitude modulation actuation. Changes in the jet flow pattern about this operating point, i.e. the carrier frequency have been studied by changing the supply voltage and the modulation frequency. The modulation frequencies have been selected on the basis of possible bursting frequencies in the approaching turbulent boundary layer and the range of the energy containing eddies inside the boundary layer for the synthetic jet based control.

It is well known fact that most of the high skin-friction regions in turbulent boundary layer are induced by near-wall streamwise vortices known as streaks and suppression in formation of these structures can lead to significant reduction in skin-friction drag. Lee et al. [20] observed that synthetic jets are more effective when the forcing frequency is in the range of T-S frequencies of the boundary layer. Significant jet effectiveness is observed at a frequency lower than the frequency at which the actuator produces the maximum velocity without cross-flow. This was attributed to the interaction of the jet with the natural destabilizing frequency of the flow. Vukasinovic et al. [18] studied both high frequency excitation and amplitude modulated synthetic jet actuation at low frequencies on the evolution of a plane free shear layer. Oscillation at low frequency (the energy containing region in the baseline power spectra) influences the mixing process by the cascade mechanism. The authors also observed profound effects on the evolution of both large and small scale motions by high frequency actuation.

Table 1
The characteristic dimensionless parameters (Re_j, L and S) of synthetic jet for unmodulated ($f_{AM} = 0$) and modulated cases at different excitation voltages (V_{exc}).

V_{exc} (V)	f_{AM} (Hz)	U_0 (m/s)	Re_j	L	S
15	0	0.1947	6.2429	0.4096	9.9569
20	0	0.3959	12.6897	0.8326	9.9569
25	0	0.5733	18.3774	1.2058	9.9569
30	0	0.8646	27.7134	1.8184	9.9569
35	0	1.0852	34.7834	2.2823	9.9569
40	0	1.5500	49.6826	3.2599	9.9569
15	10	0.7130	22.8528	1.4994	1.0210
20	10	1.3821	44.3008	2.9068	1.0210
25	10	1.9689	63.1088	4.1408	1.0210
30	10	2.5232	80.8744	5.3065	1.0210
15	25	0.6387	20.4735	1.3433	1.0210
20	25	1.1142	35.7124	2.3432	1.6143
25	25	1.7144	54.9511	3.6056	1.6143
30	25	2.2129	70.9266	4.6538	1.6143
15	50	0.4973	15.9414	1.0460	2.2830
20	50	0.8993	28.8238	1.8912	2.2830
25	50	1.2810	41.0603	2.6941	2.2830
30	50	1.8908	60.6048	3.9765	2.2830

In the present work, we are interested in the investigation of the interaction between synthetic jet and the approaching boundary layer. The literature show that the criteria for selection of modulation frequency depend on the hydrodynamic instability of base flow, i.e. the boundary layer. We have set the modulation frequency to lie within the energy containing range of the spectrum of the approaching boundary layer, in fact, close to the bursting frequency.

The displacement amplitude of the cantilever controls the peak flow rate generated by the jet. Amplitude modulation was accomplished by changing the supply voltage to the actuator over a range of 5–50 V. In addition, the high frequency carrier signal was combined with a low frequency modulating signal over a narrow range of frequencies. Fig. 2 shows the formation of a modulated signal obtained by combining the carrier signal with the modulating wave of a different amplitude and a lower frequency. The phase difference between the carrier and the modulation signal is equal to zero. This technique has been used for generating synthetic jets at frequencies other than the resonant frequency of the cantilever. The

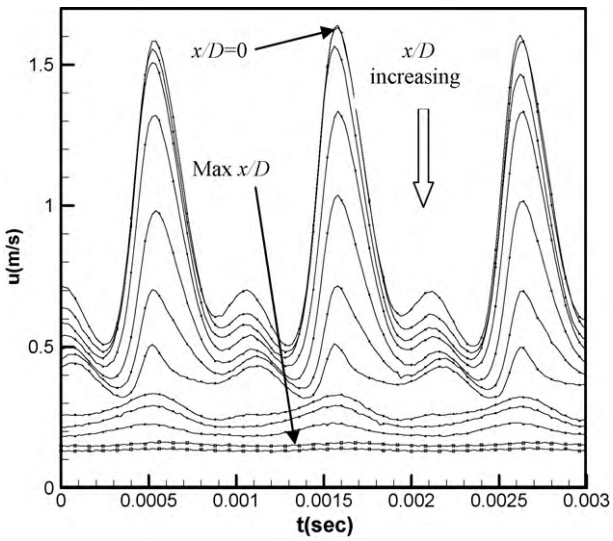

Fig. 3. Time traces of streamwise jet velocity (u) at various radial locations (x/D) with x/D ranging from 0 to 1.78 in intervals of $\Delta x/D = 0.16$ corresponding to the axial location (y/D) = 0.5. The excitation voltage is set equal to 30 V at excitation frequency of 951 Hz. The orifice diameter, D = 0.5 mm.

modulation frequencies have been set equal to 10 Hz, 25 Hz and 50 Hz. Fig. 2(a) shows the time trace of actuation voltage for the unmodulated synthetic jet at an amplitude of 20 V. Fig. 2(b)–(d) shows the time trace of the actuation voltage for the modulated case with modulation frequency equal to 10 Hz, 25 Hz and 50 Hz, respectively, at 20 V amplitude.

2.5. Dimensionless parameters

Two independent dimensionless parameters can be used for describing the synthetic jet: one is the jet Reynolds number Re_j and the other is the dimensionless stroke length L. These parameters are defined as:

$$L = \frac{L_0}{D}$$

$$Re_j = \frac{U_0 D}{\nu}$$

where U_0 is the time-averaged blowing velocity over the entire cycle of time period T, namely:

$$U_0 = \frac{1}{T}\int_0^{T/2} u_0(t)\mathrm{d}t$$

The jet stroke length, $L_0 = U_0 \times T$ represents the length of the column or slug of fluid pushed out of an orifice during the blowing stroke.

Another important parameter, the Stokes number, S is defined as

$$S = \left(\frac{2\pi Re_j}{L}\right)^{1/2}$$

The synthetic jet parameters defined above are presented in Table 1 as a function of the excitation voltage and modulation frequency. Reynolds number and stroke length can be used as measures of the strength of the synthetic jet. Table 1 shows that the jet Reynolds number and dimensionless stroke length increase with an increase in the excitation voltage for the unmodulated configuration. In comparison to the unmodulated jet at a fixed actuation voltage, there is an overall increase in the stroke length and jet Reynolds number for amplitude modulation. The stroke length and jet Reynolds number decrease with an increase in the modulation frequency at a fixed excitation voltage. Overall, the average synthetic jet characteristics results in Table 1 indicate that amplitude modulation generates a stronger synthetic jet in comparison to the unmodulated synthetic jet. Detailed characterization of the synthetic jet is presented in the later sections.

2.6. Validation experiments

The synthetic jet behavior in terms of momentum distribution during an excitation cycle is different from that of the pulsed jet. The proper formation of a synthetic jet whose mass flux over a cycle is equal to zero can be verified using the velocity time traces recorded close to the orifice exit at various radial locations. Fig. 3 presents the velocity time trace as a function of the radial coordinate (x/D). The streamwise location is close to the exit of the orifice ($y/D = 0.5$).

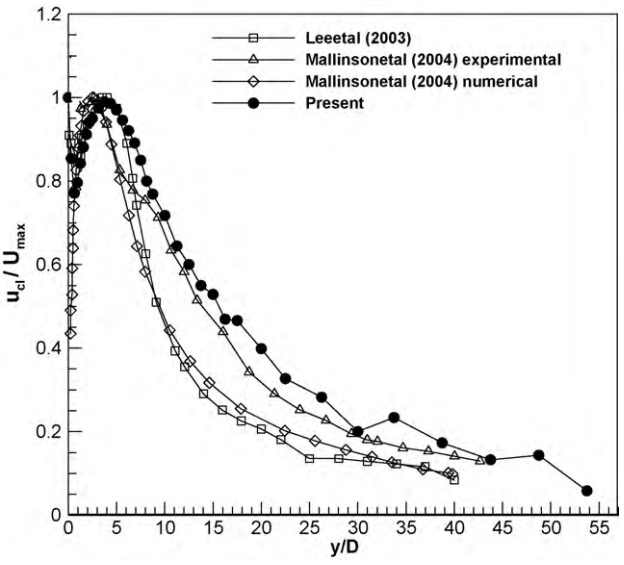

Fig. 4. Comparison of normalized jet centerline velocity (u_{cl}/U_{max}) in the axial direction (y/D) with literature. The excitation voltage amplitude is set equal to 30 V at excitation frequency of 951 Hz. The orifice diameter, $D = 0.5$ mm.

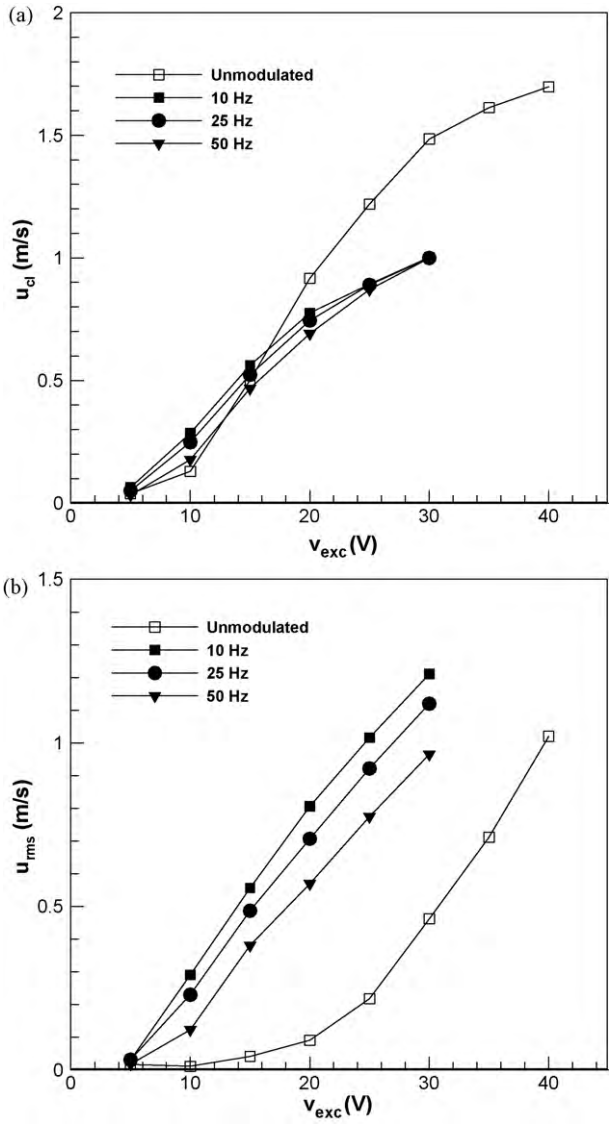

Fig. 5. Centerline mean and RMS velocities for unmodulated and amplitude modulated jets at $y/D = 2.5$ as a function of excitation amplitude for various excitation frequencies: (a) time-averaged velocity (u_{cl}) and (b) rms velocity (u_{rms}). Orifice diameter $D = 0.5$ mm and carrier frequency is equal to 951 Hz.

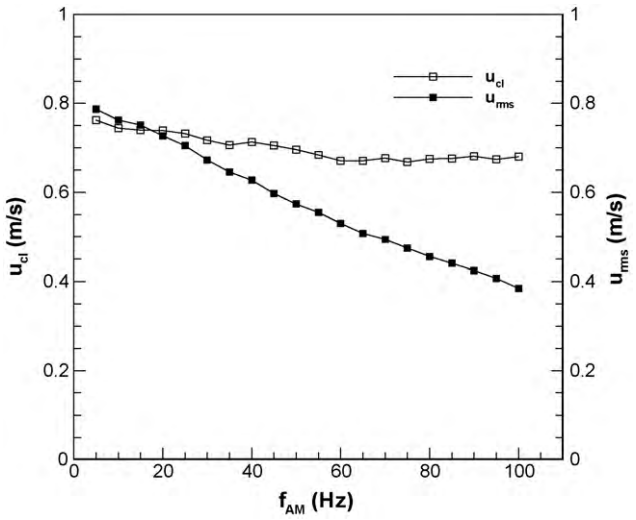

Fig. 6. Variation of jet centerline mean (u_{cl}) and rms velocities (u_{rms}) as a function of modulation frequency at an axial location, $y/D = 2.5$ for excitation amplitude, $V_{exc} = 20$ V. Orifice diameter, $D = 0.5$ mm and carrier frequency is equal to 951 Hz.

An excitation voltage of 30 V is considered. Since the hotwire measurements are not sensitive to the direction of flow, flow reversal is seen as a second peak in Fig. 3. Flow reversal is sustained up to a considerable radial distance. The peak during reversal, i.e. suction is lower compared to the blowing phase, mainly owing to a change in effective cross-sectional area during the two phases. The time duration of acceleration of the synthetic jet is smaller than that of jet retardation. The second peak near the orifice disappears as we move away in the radial direction. The flow towards the cavity during the suction stroke is a maximum near the center of the orifice. It reduces in the radial direction due to the influence of ambient static fluid. Consequently, the two peak structure vanishes and only one small peak is observed during one oscillation cycle. Similar velocity time traces for an unmodulated synthetic jet have been presented by Utturkar et al. [21].

Fig. 4 compares the normalized axial velocity profile at the centerline of the jet with that in the literature. The jet centerline velocity increases in the axial direction to a peak value with subsequent reduction to zero velocity in the ambient. The normalized profile in Fig. 4 matches reasonably well with the experimental

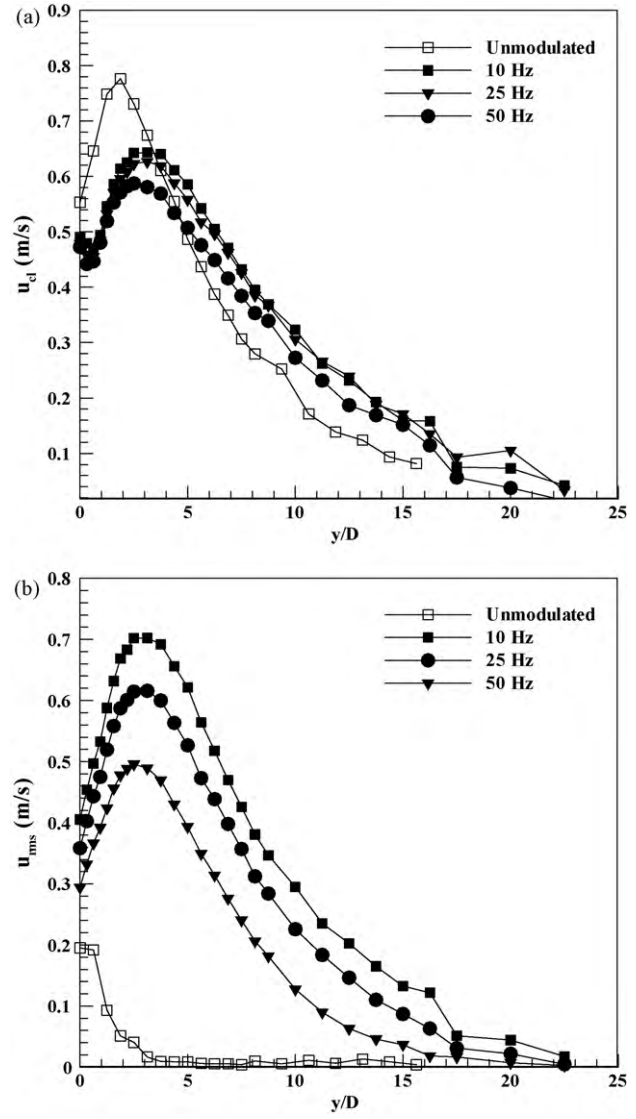

Fig. 7. Jet centerline velocity profiles in the axial (y/D) direction for unmodulated and modulated jets: (a) time-averaged velocity (u_{cl}), and (b) rms velocity (u_{rms}). Orifice diameter, $D = 0.5$ mm and carrier frequency is equal to 951 Hz.

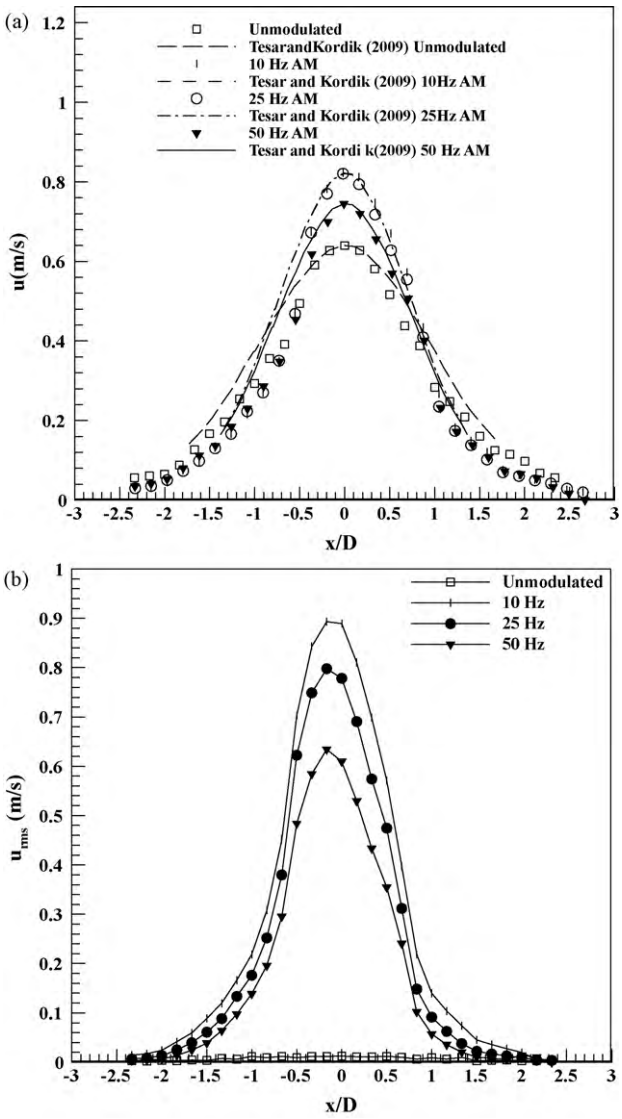

Fig. 8. Jet velocity profiles in the radial direction for unmodulated and modulated jets at axial location, $y/D = 6$: (a) time-averaged velocity (u), and (b) RMS velocity (u_{rms}). Orifice diameter, $D = 0.5$ mm and carrier frequency is equal to 951 Hz.

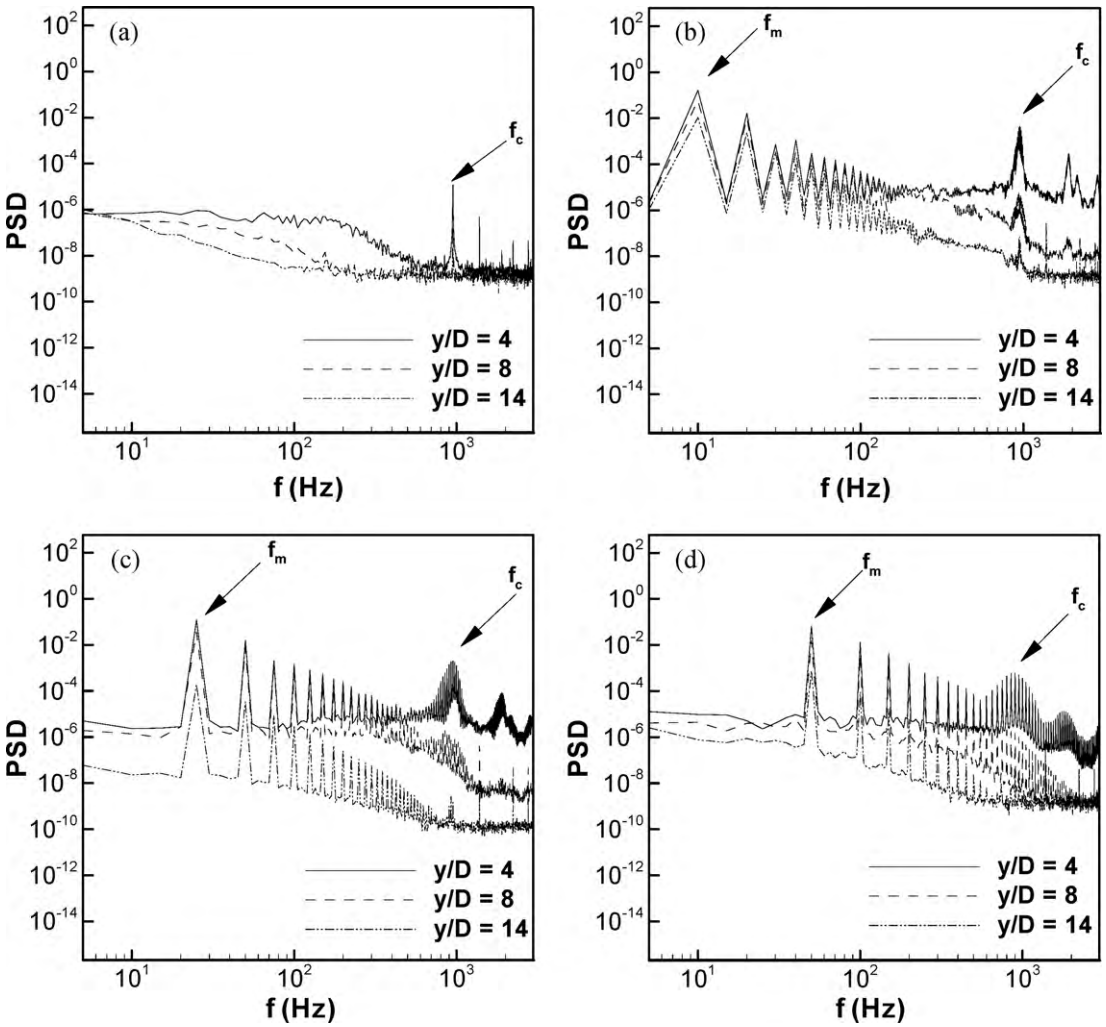

Fig. 9. Velocity power spectra at V_{exc} = 20 V for different axial locations (y/D = 4, 8, 14) at the jet centerline (x/D = 0): (a) Unmodulated jet, (b) AM at f_{AM} = 10 Hz, (c) AM at f_{AM} = 25 Hz, and (d) AM at f_{AM} = 50 Hz. Orifice diameter, D = 0.5 mm and carrier frequency is equal to 951 Hz.

results of Mallinson et al. [22]. The slight mismatch in the downstream region ($y/D > 10$) with that of Lee et al. [20] can be attributed to the difference in the jet Reynolds number between the two studies. Compared to 0.776 m/s of the present study, the maximum jet centerline velocity of the synthetic jet used by Lee et al. [20] is equal to 5 m/s. The diameter of the orifice being equal to 0.5 mm for the two studies, it can be concluded that the differences are related to those in the jet Reynolds number. Overall, Figs. 3 and 4 validate the exit-plane properties of the synthetic jet of the present study.

3. Results and discussion

Synthetic jets are characterized by the formation, advection, and diffusion of vortex rings. The strength of the vortex ring can be gauged in terms of circulation while its frequency content determines the likely impact when the synthetic jet is combined with a second flow field that needs to be controlled. The vortex rollup characteristic of synthetic jet is strongly influenced by the nature of excitation of the diaphragm. The present study examines the effect of excitation voltage and modulation frequency on the characteristics of the synthetic jet. The influence of the orifice diameter and the presence of a neighbor on the evolution of the synthetic jet have also been investigated. Results are presented in terms of the time-averaged velocity profiles in the axial and the radial directions, velocity power spectra and time series, and flow visualization using the schlieren technique.

3.1. Effect of excitation voltage and modulation frequency

Fig. 5 presents the time-averaged centerline velocity and the corresponding rms velocity as a function of the excitation voltage at an axial location of y/D = 2.5 from the exit plane of the orifice. Both unmodulated and modulated jets are considered at various modulation frequencies. The excitation voltage is varied between 5 V and 40 V. Since the dielectric breakdown of the piezo patch occurs at 80 V (peak-to-peak), the maximum excitation voltage for the amplitude modulation experiment is set equal to 40 V.

Fig. 5 shows an increase in both the time-averaged and the rms velocities with an increase in the excitation voltage. The centerline velocity quantities are nearly equal for the unmodulated and modulated experiments till an excitation voltage of 15 V is reached. Subsequently, the time-averaged velocity decreases with the excitation voltage for the modulated case. In comparison to the unmodulated jet, however, the rms velocity is greater for all amplitude modulation experiments, increasing with the excitation voltage (Fig. 5(b)). The rms velocity decreases at all exci-

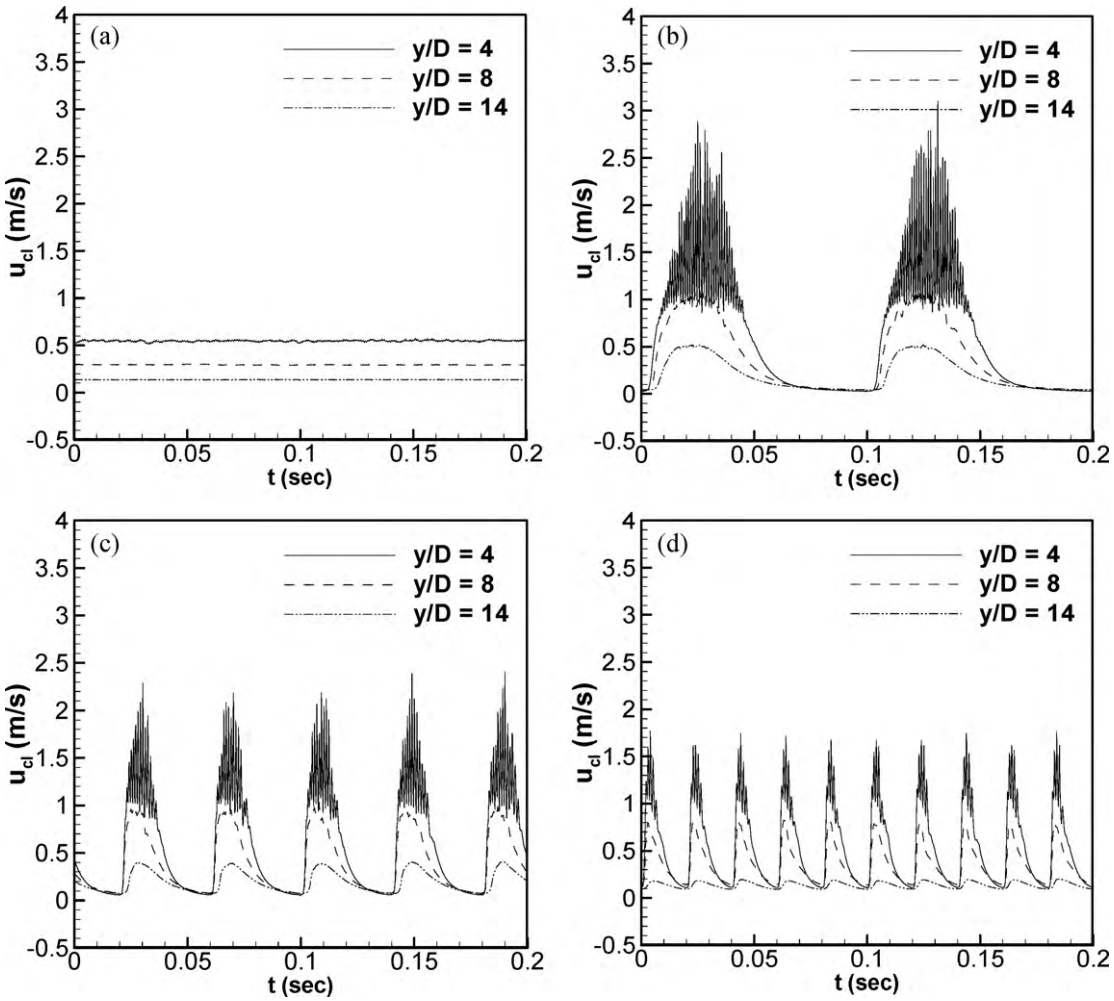

Fig. 10. Velocity time traces at V_{exc} = 20 V for various axial locations (y/D = 4, 8, 14) at the orifice centerline (x/D = 0): (a) Unmodulated jet, (b) AM at f_{AM} = 10 Hz, (c) AM at f_{AM} = 25 Hz, and (d) AM at f_{AM} = 50 Hz. Orifice diameter, D = 0.5 mm and carrier frequency is equal to 951 Hz.

tation voltages with an increase in modulation frequency. This behavior is related to the variation of the stroke length of the synthetic jet with respect to the modulation frequency (Table 1). For unmodulated and amplitude modulated jets, the stroke length increases with an increase in the excitation voltage. The stroke length decreases with an increase in frequency. The stroke length represents the length of the fluid column containing the fluid that is ejected during the blowing phase. It is proportional to the distance traveled by the vortex ring from the orifice exit till the onset of the next suction cycle. When the stroke length is small, the vortex ring does not move sufficiently far away from the orifice exit. It is drawn back into the orifice during the suction stroke. For the higher modulation frequency jets, the ejection period is smaller and therefore the vortex ring has less time to grow. As a result, the rms velocity fluctuations are uniformly smaller.

The effect of modulation frequency on the jet characteristics is presented in Fig. 6. Quantities reported are the time-averaged and the rms velocity variation along the jet centerline. The modulation frequencies are varied from 5 Hz to 100 Hz at a constant excitation voltage of 20 V and amplitude modulation level of 100%. With an increase in modulation frequency, Fig. 6 shows a reduction in the magnitude of both the time-averaged and the rms velocities. For an increase in the modulation frequency, the relative reduction in the rms velocity is much greater than the time-average. This trend indicates a greater influence of amplitude modulation at lower frequencies when compared to the higher. As noted in Table 1, the reason can be traced to a smaller stroke length at higher frequencies. A confirmation of this result using flow visualization is presented in Section 3.6.

3.2. Axial and radial velocity distribution

The evolution of the synthetic jet in the axial direction depends on the vortex rollup and its interaction with the neighboring field. Fig. 7 compares the time-averaged and rms velocities in the axial direction for the amplitude modulated jet with respect to the unmodulated. The excitation voltage is set equal to 20 V and three modulation frequencies 10 Hz, 25 Hz and 50 Hz are compared. Fig. 7 shows that the time-averaged and rms velocities increase in the axial direction to a peak and subsequently decrease. The highest peak in the time-averaged velocity is observed for the unmodulated jet at an earlier axial (y/D) location. The peak position shifts away from the orifice with modulation. The peak velocity for the modulated jet decreases with an increase in modulation frequency.

When compared to the unmodulated, the rms velocity is significantly higher for the modulated jet (Fig. 7(b)). The axial location (y/D) corresponding to the peak rms velocity is independent of frequency. However, the peak value is dependent on the modulation frequency itself. This trend is clearly brought out through power spectra in Section 3.5.

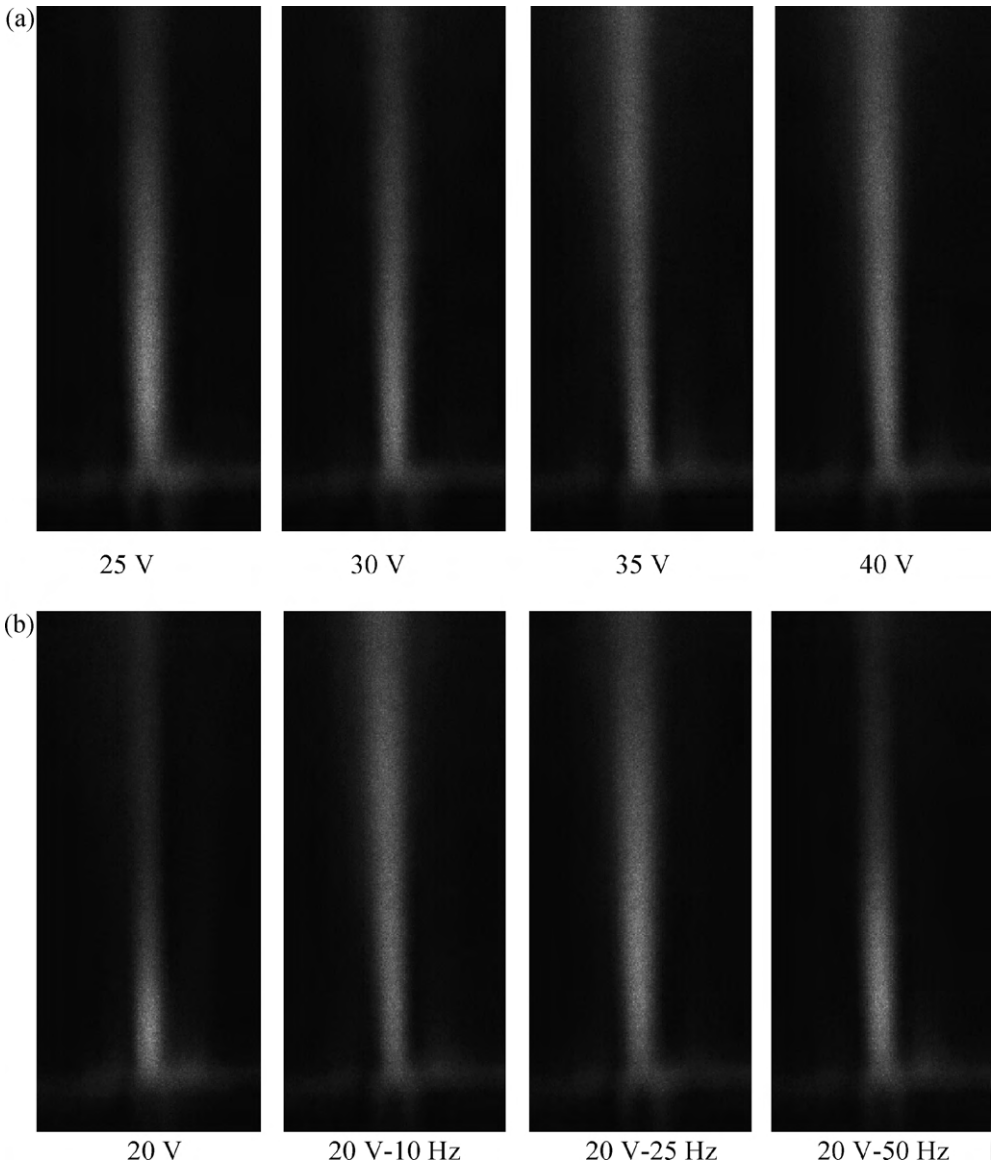

Fig. 11. Schlieren images of a synthetic jet as a function of (a) excitation amplitudes and (b) modulation frequency. Orifice diameter, $D = 0.5$ mm and carrier frequency is equal to 951 Hz.

The spatial growth of the synthetic jet due to mixing with the ambient fluid is investigated in terms of the radial velocity distribution. Fig. 8 compares the radial velocity profile at an axial location of $y/D = 6$ for the unmodulated and modulated cases. The overall nature of the time-averaged and rms velocity profiles is identical, with a maximum at the jet centerline and a reduction in its magnitude in the radial direction. The highest peak in the time-averaged velocity is observed for an amplitude modulated jet at the lowest frequency and the minimum centerline velocity is observed for the unmodulated jet (Fig. 8(a)). Fig. 8(a) also compares the radial velocity distribution from the present study with that from quasi-similarity model of Tesař and Kordík [14]. There is a good match between the experiment and the quasi-similarity model indicating general similarity in behavior between the modulated and the unmodulated synthetic jets. In contrast, the rms velocity for the unmodulated jet is significantly lower than that of the modulated jet (Fig. 8(b)). At all radial locations, the overall rms velocity is higher for modulation at lower frequencies when compared to higher modulation frequencies. The influence of the modulation frequency is higher near the jet centerline when compared to its periphery. The overall jet width is also higher at low frequencies.

3.3. Velocity power spectra and time traces

Fig. 9 compares the power spectra of the streamwise velocity component of the unmodulated and modulated jets. The excitation voltage is set equal to 20 V and three modulation frequencies, namely 10 Hz, 25 Hz, and 50 Hz have been compared. Power spectra have been determined from velocity measurements along the orifice centerline and are shown at three axial locations ($y/D = 4$, 8, and 14). Various axial (y/D) locations have been considered for understanding the distribution of frequency content in the flow field. A re-distribution in energy among the harmonics is expected due to vortex evolution and interaction. The axial location, $y/D = 4$ corresponds to the peak rms velocity and downstream points $y/D = 8$ and 14 correspond to the decay region of the rms velocity (Fig. 7).

Fig. 9(a) shows a clear spectral peak at the resonant frequency of the actuator (=951 Hz) for the unmodulated jet. The low fre-

quency portion of the power spectrum originates from the large scale structures of the flow and contributes strongly to the kinetic energy of fluctuations. Fig. 9(a) shows that the energy containing region diminishes in magnitude in the axial direction, correlating well with a reduction in the rms velocity of Fig. 7. With increase in the axial distance from the orifice, the low frequency part of the spectrum attenuates quite rapidly, indicating an early break-up of the ring vortices produced by the tip of the orifice. The power spectra of the amplitude modulated synthetic jets are shown in Fig. 9(b)–(d). The corresponding frequencies are in the range of 10–50 Hz, being much smaller than 951 Hz, the carrier frequency. The spectra in Fig. 9(b)–(d) show a clear peak at the respective dominant frequencies. Additional peaks of lower value are also to be seen at integer multiples of the modulating frequency. In contrast to the unmodulated jet, sidebands appear around peak, and thus the bandwidth of the peak at the modulation frequency increases in the axial direction, indicating the broadening of the energy containing region. For the unmodulated jet, the sharp peak at the resonant frequency remains unchanged in the streamwise direction.

Fig. 9 shows that the total areas under the respective spectra are higher for the amplitude modulation jet in comparison to the unmodulated. These areas diminish in the axial direction. The relative distribution of power between the low frequency and the high frequency regions depends on the modulation frequency. When the modulation frequency is close to the frequency of the energy containing eddies of the unmodulated jet (Fig. 9(a)), a significant influence is seen in the jet evolution, particularly in terms of velocity fluctuations and distribution of energy over the frequency scale. The increase in frequency content of the energy containing eddies is evident from the broadening of the power spectra for the modulated jet. The shift in the position of the peak itself reveals that the size of the freshly created large eddies is affected by the presence of smaller ones in the flow field.

Fig. 10 shows the time traces of the streamwise component of velocity corresponding to the power spectra of Fig. 9. The highest peak velocity for the amplitude modulated jet is observed at the minimum frequency considered, namely 10 Hz (Fig. 10(b)). The peak velocity magnitude decreases with an increase in the magnitude of the modulation frequency, Fig. 10(c) and (d), consistent with the result that the velocity fluctuations of the unmodulated jet are smaller than the modulated jet (Figs. 5 and 7). The carrier frequency content (at 951 Hz) is strongly attenuated in the downstream region and the fluctuation at the modulation frequency alone (namely 10–50 Hz) is significant. These data of Fig. 10 are in agreement with the spectra of Fig. 9. The time traces of velocity in Fig. 10 show greater periodicity at the modulation frequency over a considerable axial distance.

The modulated and unmodulated voltage signals that drive the synthetic jet actuator are shown in Fig. 2. Here, the peak voltages of all signals are seen to be nearly equal. In contrast, the velocity peaks created in the jets vary from one actuation condition to another. Further, these peaks decay in the axial direction. An examination of Fig. 9 provides an explanation for these trends. The velocity peak corresponds to the modulation frequency (except for the unmodulated jet, where it corresponds to the carrier frequency). The peak value can be associated with a vortex ring created by the fluid leaving the orifice. The vortex advects in the streamwise direction and is progressively broken up in such a way that harmonics of the modulation frequency are to be seen in the power spectra. A new vortex is then created in a subsequent cycle when smaller vortices are already present in the flow field. The new vortex, then has a size different from the one created in the purely quiescent fluid. This scenario contrasts with an unmodulated jet where carrier frequency is high, the initial vortex generated is small, which dissipates rapidly with distance.

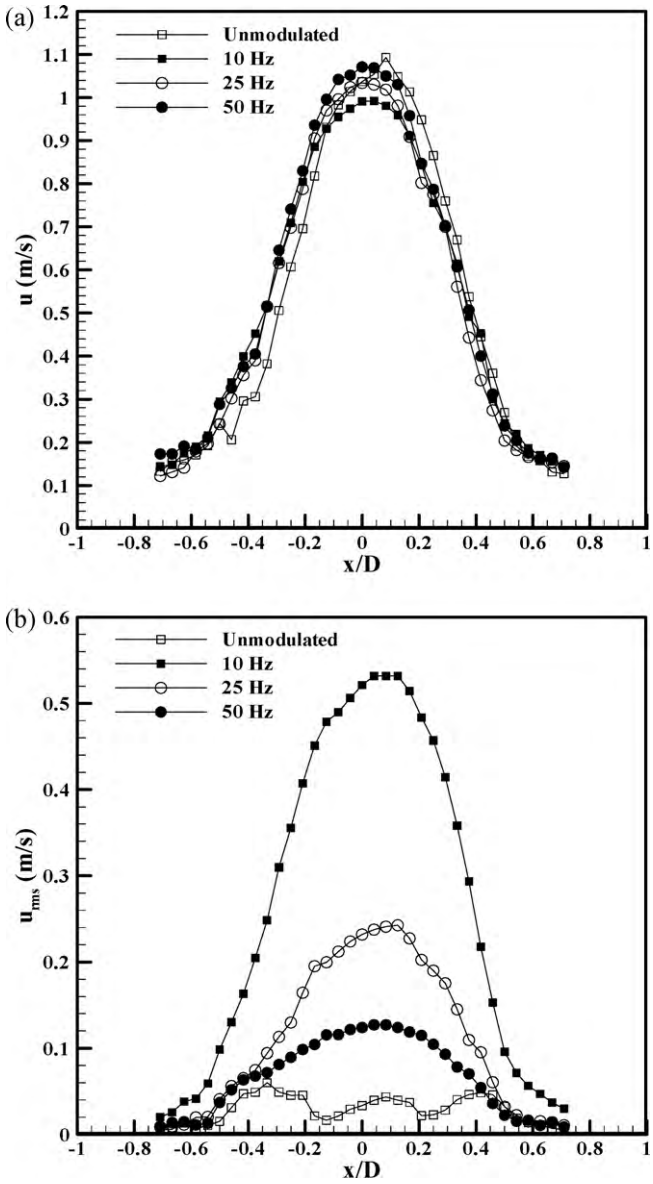

Fig. 12. (a) Time-averaged radial velocity (u) and (b) radial rms velocity (u_{rms}) profile for larger diameter (D = 2 mm) orifice at the streamwise location, y/D = 1.5 for various excitation conditions. The carrier frequency is equal to 475 Hz.

Hence, all later vortices are created practically in a stationary fluid.

3.4. Schlieren visualization

Fig. 11(a) shows the time-averaged schlieren images of the synthetic jet as a function of excitation voltage in the range of 25–40 V. The streamwise extent of the synthetic jet is seen to increase with an increase in the excitation voltage. These results correlate well with the stroke length data of Table 1, where the stroke length is shown to increase with the excitation voltage. Fig. 5(a) also shows an increase in jet centerline velocity with increase in the excitation voltage, thus providing an explanation for the increased spread in the main flow direction.

Fig. 11(b) shows the time-averaged schlieren images as a function of the modulation frequency (10 Hz, 25 Hz, and 50 Hz) at an excitation voltage of 20 V. The average length of the amplitude modulated jet is higher in comparison to that of the unmodulated jet. Fig. 7(a) also supports the above claim that the jet penetra-

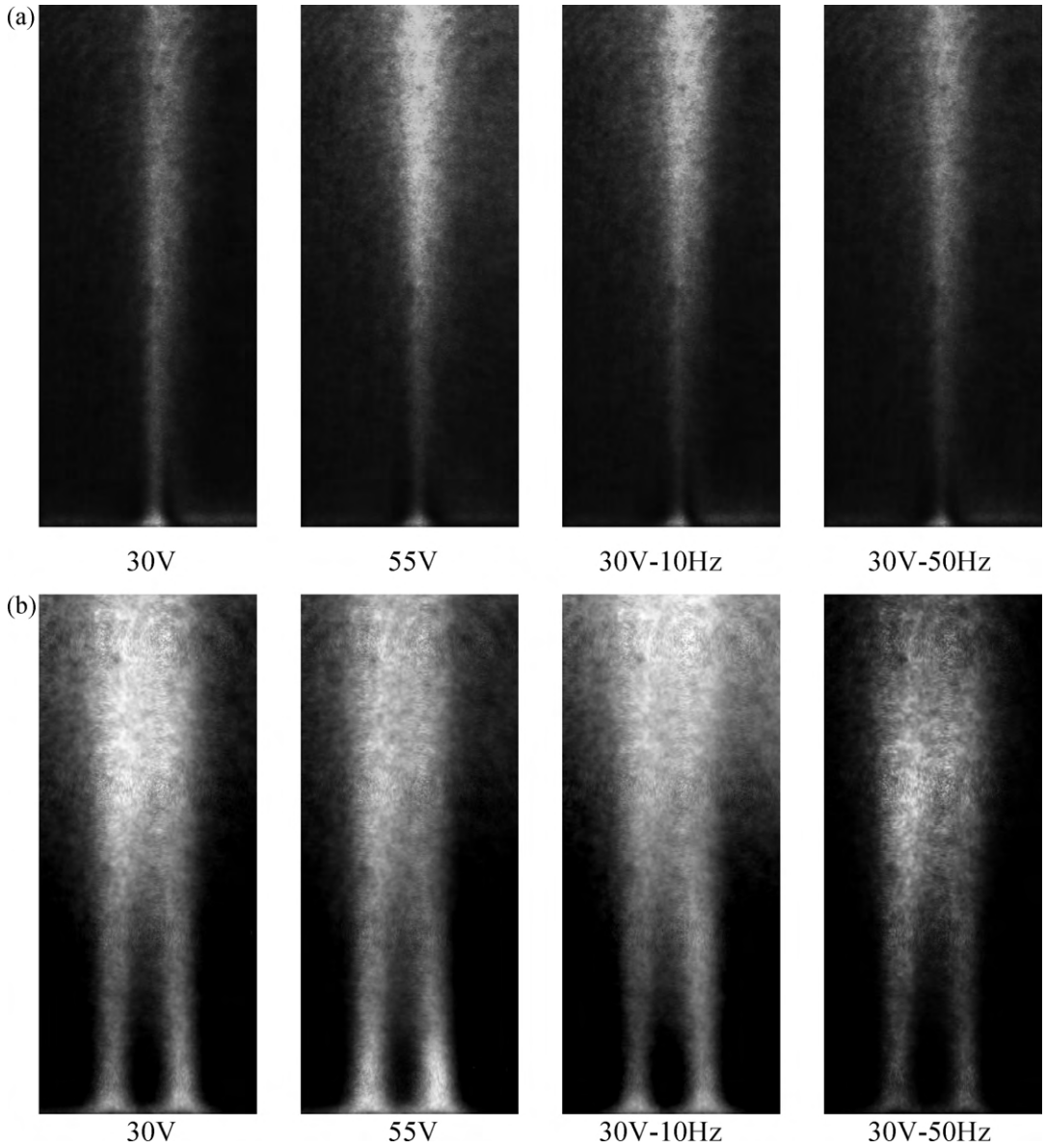

Fig. 13. Time-averaged Schlieren images for (a) single jet, and (b) double jets under different excitation conditions. Orifice diameter, $D = 2$ mm for all jets and the distance between the jets for double jet configuration is equal to 4 mm. The carrier frequency is equal to 475 Hz.

tion length for an unmodulated excitation is lower when compared to the modulated since the centerline velocity beyond $y/D > 15$ is insignificant for the former when compared to the latter. In addition, the higher rms velocity for the modulation experiment beyond $y/D > 5$ in comparison to the unmodulated, strengthens the above claim (Fig. 7 (b)). At 10 Hz amplitude modulation frequency, the penetration depth of the jet is about $16\times D$ compared to $9\times D$ value at 50 Hz amplitude modulation frequency. Thus, the jet penetration length decreases with an increase in the modulation frequency. Once again, these results correlate well with the stroke length data of Table 1 and the centerline velocity variation in Fig. 6. Overall, Fig. 11 confirms the effectiveness of amplitude modulation for modification of the synthetic jet characteristics. For a given excitation voltage, the strength of the jet can be increased by employing low frequency modulation.

3.5. Effect of orifice diameter

The orifice diameter of the synthetic jet was changed from 0.5 mm to 2 mm to investigate the consistency of the amplitude modulation effect. Fig. 12 compares the radial distribution of the time-averaged and rms velocities for unmodulated jets and those with amplitude modulation for the larger orifice diameter ($D = 2$ mm). As discussed in Section 3.4, the time-averaged velocity is insensitive to amplitude modulation though the rms velocity distribution shows a strong influence. The effect is stronger at lower modulation frequencies, since rms values decrease from 10 Hz onwards to 50 Hz. These results were also uniformly seen at the smaller orifice diameter ($D = 0.5$ mm) presented earlier. Fig. 13(a) presents schlieren images of the jet emerging from the larger orifice for various excitation amplitudes and frequencies. The overall spread and size of the jet is larger for the synthetic jet with larger orifice in comparison to that of the small sized orifice seen in Fig. 11. Fig. 13 shows the jet strength to increase with excitation voltage while low frequency modulation is more effective when compared to the higher frequency. Comparing Fig. 13 with Fig. 8 for the smaller orifice, the influence of amplitude modulation for the two orifice diameters is seen to be similar. Overall, jet patterns recorded for the orifices of two different diameters are found to be qualitatively similar.

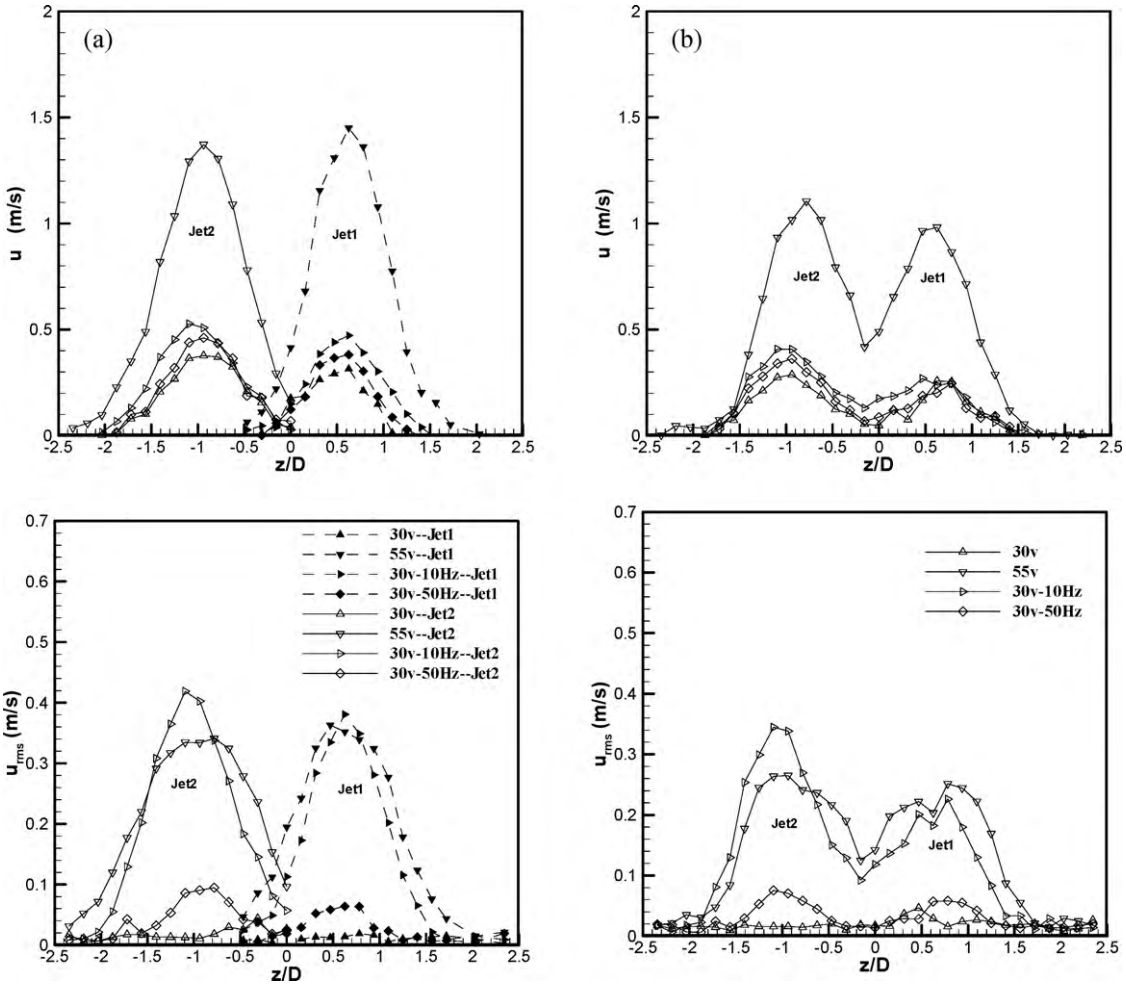

Fig. 14. Time-averaged radial velocity (u) and radial rms velocity (u_{rms}) profile in the spanwise direction (Z/D) at the axial location $y/D = 3$ for various excitation conditions and jet operations: (a) either jet 1 (solid lines) or jet 2 (broken lines) operating, and (b) both jet 1 and jet 2 running simultaneously. The orifice diameter, $D = 2$ mm and the distance between the jets is equal to 4 mm. The carrier frequency is equal to 475 Hz.

3.6. Double jet configuration

The number of synthetic jets placed adjacent to each other is an additional parameter for optimization in flow control applications. The present section is concerned with the influence of amplitude modulation in a double jet configuration with a pitch-to-diameter ratio equal to 2. Fig. 13 shows visualization images using schlieren for both single and double jet configurations at various modulation frequencies. The orifice diameters are equal for the jets, being $D = 2$ mm while the distance between the two jets is 4 mm. In the near field region, the two jets evolve independently of each other. The two jets grow in the downstream direction and merge with each other. The width of the dual jet configuration is greater than twice those of the individual synthetic jets (Fig. 13(b)). This result indicates an increase in the effectiveness of the dual jet and the occurrence of strong interaction between them.

Fig. 14 presents the radial u (time-averaged) and u_{rms} profiles for the single and double jet configurations. Fig. 14(a) shows the highest average fluid speed at an actuation of 55 V, when jet 1, jet 2 and the two-jet configuration are considered. The synthetic jet characterization plot of Fig. 5 also shows a higher u-velocity for the unmodulated jet excited at 55 V. Fig. 14(b) shows lower average jet velocity for the double jet configuration in comparison to the single jet actuation. This result can be attributed to greater mixing of the vortices generated by the two actuators and hence a reduction in the peak value. No significant influence of amplitude modulation on the u-velocity is observed, either for the single jet or the dual jet configuration. Amplitude modulation affects the rms velocity, for example, at an amplitude of 30 V and 10 Hz modulation frequency shows comparable rms velocity as that of 55 V without modulation. The inter-jet region shows higher u and u_{rms} velocities for the dual jet configuration in comparison to the single jet. Overall, Fig. 14 confirms the broadening of the two-jet system.

Fig. 15 presents the u' spectra of one of the jets (jet 1) at various spanwise locations ($z/D = -0.31$ and -0.47) for a wall normal location of $y/D = 3$ and various actuation conditions. Comparing Fig. 15(a) and (b) indicates a significant influence of excitation voltage in the energy containing region of the power spectra. The carrier frequency is clearly visible in all spectra. Fig. 15(a) shows the slope of the spectra for single and dual jets to be significantly different at the two locations, namely $z/D = -0.31$ and -0.47. There is an additional broad peak at $z/D = -0.47$ for the dual jet configuration. This is indicative of the generation of additional energy containing eddies due to the interaction between the two jets. A comparison of Fig. 15(c) and (d) reveals the difference in the influence of the modulation frequency on the energy containing eddies. Lower modulation frequency leads to fuller spectra in the low frequency range. The dual jet configuration shows a larger slope in the dissipation regime because the jet interaction produces smaller vortices and hence greater viscous dissipation. A comparison of Fig. 15(b) and (c) indicates similarity in the average energy content at an excitation of 55 V (unmodulated) and 30 V, 10 Hz modulation fre-

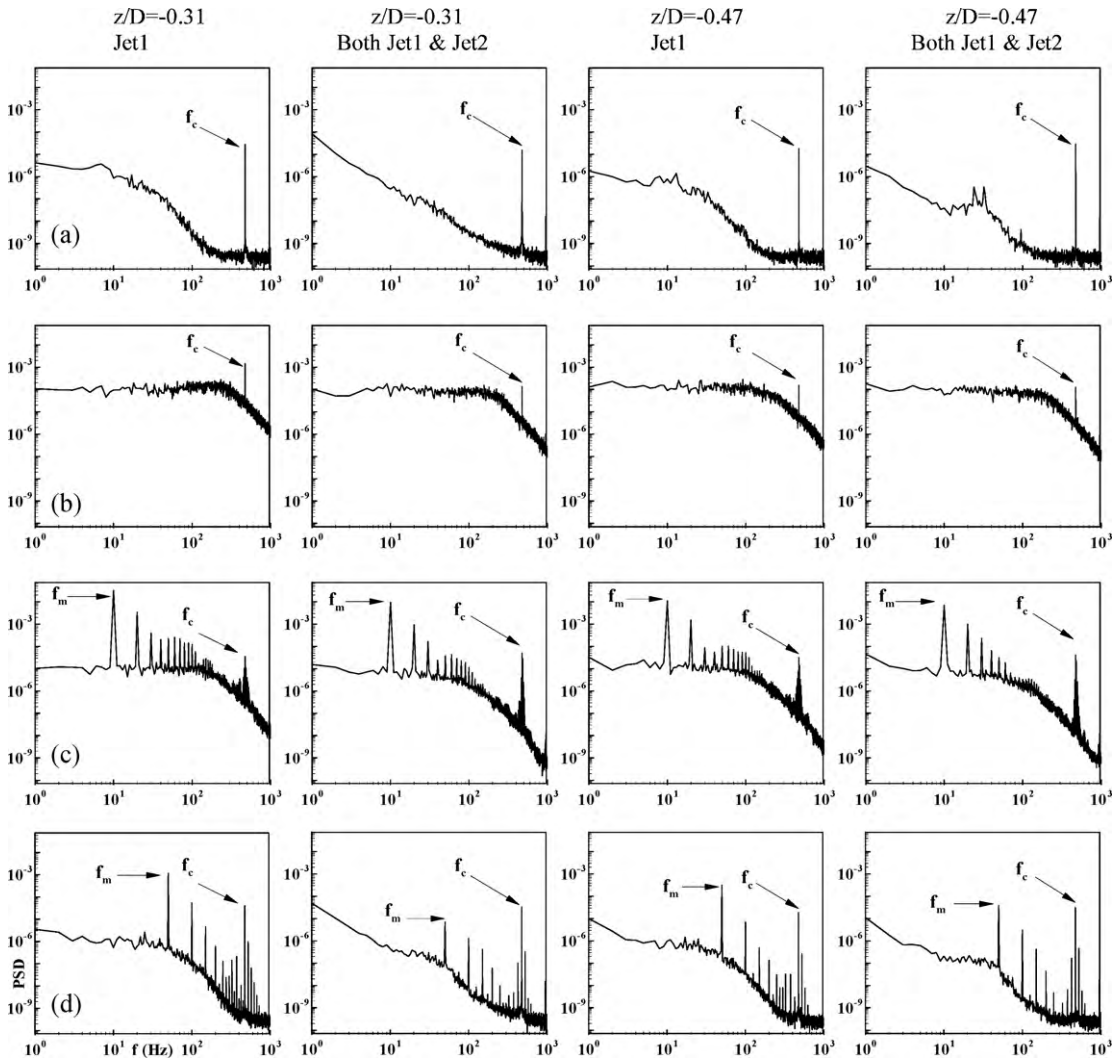

Fig. 15. The u' spectra at different spanwise (Z/D) locations of the jet (jet 1) at axial location $y/D = 3$ with both single jet (jet 1) and double jet (jet 1 and jet 2) operating under various actuation conditions: (a) $V_{exc} = 30$ V, (b) $V_{exc} = 55$ V, (c) $V_{exc} = 30$ V, $f_{AM} = 10$ Hz, and (d) $V_{exc} = 30$ V, $f_{AM} = 50$ Hz. The orifice diameter, $D = 2$ mm and the distance between the jets is equal to 4 mm. The carrier frequency is equal to 475 Hz.

quency with the exception that additional frequencies are seen for the modulated jets. Fig. 15 supports the rms velocity trends shown in Fig. 14. Thus, the effect of amplitude modulation and the interaction between two jets can be clearly observed from the spectra of Fig. 15.

4. Conclusions

A synthetic jet actuator using cantilever-type piezo-actuation has an inherent limitation since it provides maximum amplitude of displacement only at its resonant frequency. Amplitude modulation provides a mechanism by which additional frequency can be introduced as a control parameter of the synthetic jet actuator while the amplitude of the cantilever vibration is increased. In applications, the modulation frequency of the synthetic jet can be tuned with that of the main flow being controlled. The present study investigates the characteristics of the synthetic jet for a carrier frequency of 951 Hz under modulation conditions varying from 10 Hz to 50 Hz. Hotwire anemometry and schlieren visualization techniques have been used. Of specific interest is the effect of amplitude modulation at various frequencies and interaction between two neighboring synthetic jets. Important observations arrived at in the present investigation are summarized below.

1. Amplitude modulation strongly influences the basic characteristics of a synthetic jet. The extent of influence depends on the selection of modulation frequency.
2. The non-dimensional stroke length of the synthetic jet increases with actuation voltage. The stroke length is higher for amplitude modulation compared to that of an unmodulated jet. The increase in the stroke length is higher at lower modulation frequencies.
3. Amplitude modulation increases both the jet penetration in the streamwise direction and the magnitude of rms velocity fluctuations. Low frequency modulation resonates with the base (vortical) flow of the unmodulated jet and broadens the energy containing region of the power spectrum.
4. Schlieren visualization reveals the spatial spread and distribution of the jets and confirms the stronger influence of amplitude modulation on growth of the synthetic jet.
5. The dual jet configuration in which the main jet grows in the presence of a neighboring synthetic jet results in joint improvement of the combined growth rate.

Appendix A. Supplementary data

Supplementary data associated with this article can be found, in the online version, at doi:10.1016/j.sna.2010.05.008.

References

[1] B.L. Smith, A. Glezer, Vectoring and small scale motions affected in free shear flows using synthetic jet actuators, in: AIAA 35th Aerosp. Sci. Meet., Paper no. AIAA 97-0213, 1997.
[2] B.L. Smith, A. Glezer, The formation and evolution of synthetic jets, Phys. Fluids 21 (1998) 2281–2297.
[3] L.D. Kral, J.F. Donovan, A.B. Cain, A.W. Cary, Numerical simulation of synthetic jet actuators, in: AIAA 28th Fluid Dyn. Conf., Paper no. AIAA 97-1824, 1997.
[4] D.P. Rizzetta, M.R. Visbal, M.J. Stanek, Numerical investigation of synthetic jet flow fields, AIAA J. 37 (8) (1999) 919–927.
[5] S.G. Mallinson, G. Hong, J.A. Reizes, Some characteristics of synthetic jets, in: AIAA 30th Fluid Dyn. Conf., Paper no. AIAA 97-1792, 1999.
[6] E. Cater, J. Soria, The evolution of round zero net mass flux jet, J. Fluid Mech. 472 (2002) 167–200.
[7] B.L. Smith, G.W. Swift, A comparison between synthetic jets and continuous jets, Exp. Fluids 34 (2003) 467–472.
[8] S. Ugrina, A. Flatau, Investigation of synthetic jet actuator design parameters, Proc. SPIE 5390 (2004) 284–296.
[9] S.R. Fugal, B.L. Smith, R.E. Spall, Displacement amplitude scaling of a two-dimensional synthetic jet, Phys. Fluids A 17 (2005) 045103.
[10] F. Cannelle, M. Amitay, Synthetic jets: spatial evolution and transitory behavior, in: 43rd AIAA Aerospace Sciences Meeting and Exhibit, 2005.
[11] Z. Trávníček, V. Tesař, A.B. Wang, Enhancement of synthetic jets by means of an integrated valve-less pump. Part 1. Design of the actuator, Sens. Actuators A 120 (2005) 232–240.
[12] J.L. Xu, J. Sha, C.F. Lin, K.Y. Zhang, PIV experimental research of instantaneous flow characteristics of circular orifice synthetic jet, J. Hydrodyn. 19 (2006) 453–458.
[13] M.D.C. Gaetano, I. Gaetano, On the near field of an axisymmetric synthetic jet, Fluid Dyn. Res. 39 (2007) 673–693.
[14] V. Tesař, J. Kordík, Quasi-similarity model of synthetic jets, Sens. Actuators A 49 (2009) 255–265.
[15] G. Hong, Effectiveness of micro synthetic jet actuator enhanced by flow instability in controlling laminar separation caused by adverse pressure gradient, Sens. Actuators A 132 (2006) 607–615.
[16] B.D. Ritchie, J.M. Seitzman, Acetone mixing control of fuel jets using synthetic jet technology; scalar field measurements, AIAA paper 99-0448, 1999.
[17] R. Rathnasingham, K.S. Breuer, Active control of turbulent boundary layers, J. Fluid Mech. 495 (2003) 209–233.
[18] B. Vukasinovic, D.G. Lucas, A. Glezer, A direct manipulation of small-scale motions in a plane shear layer, AIAA paper 2004-2617, 2004.
[19] S. Margalit, D. Greenblatt, A. Seifert, I. Wygnanski, Delta wing stall and roll control using segmented piezoelectric fluidic actuators, J. Aircraft 42 (3) (2005) 698–709.
[20] C. Lee, H. Guang, Q.P. Ha, S.G. Mallinson, A piezoelectrically actuated micro synthetic jet for active flow control, Sens. Actuators A 108 (2003) 168–174.
[21] Y. Utturkar, M. Arik, C.E. Seeley, M. Gursoy, An experimental and computational heat transfer study of pulsating jets, ASME J. Heat Transf. 130 (2008), 6 2201-(1-10).
[22] S.G. Mallinson, J.A. Reizes, G. Hong, P.S. Westbury, Analysis of hot-wire anemometry data obtained in a synthetic jet flow, Exp. Therm. Fluid Sci. 28 (2004) 265–272.

Biographies

Adnan Qayoum is working as a faculty in mechanical engineering department at National Institute of Technology Srinagar from 1993. He received his M.E. degree in mechanical engineering from University of Roorkee, India in 1999. Since 2005, he is a Ph.D. student at Indian Institute of Technology Kanpur. His interest and subject of Ph.D. studies are heat transfer enhancement in a serpentine duct using synthetic jet and permeable ribs.

Mr. Vaibhav Gupta completed his B.Tech. degree with honors from Madhav Institute of Technology and Science, Gwalior, MP in year 2006. He subsequently completed his M.Tech. degree in mechanical engineering from IIT Kanpur in year 2008. He is currently working as an engineer in Engineering Research Center, TATA Motors, Pune.

Dr. P.K. Panigrahi did his Ph.D. and M.S. in mechanical engineering from LSU, Baton Rouge, USA. He has been working as a faculty in the mechanical engineering department of IIT Kanpur since 8th January 1998. Dr. Panigrahi's research focuses on development of state-of-the-art experimental techniques preferably using lasers and detectors/sensors to analyze complex flow fields. The other area of his interest is development of various flow control strategies with overall emphasis on improving the performance of various engineering devices and processes.

Dr. K. Muralidhar is a Ph.D. from University of Delaware, USA. He has conducted experiments and numerical simulation in applications related to fluid mechanics, heat and mass transfer. He has contributed to the understanding of transport phenomena in porous media, wake dynamics, development of numerical algorithms, and laser measurement of flow and thermal fields. His research finds applications in industrial processes such as enhanced oil recovery, regenerators, nuclear waste disposal, growth of optical crystals and CVD reactors. He is presently on the faculty of IIT Kanpur (India).